SUPPLEMENTARY MATERIAL

Fluoxetine exerts anti-inflammatory effects on human epidermal keratinocytes and suppresses their endothelin release

Kinga Fanni Tóth,[1,2] Dorottya Ádám,[1,2] József Arany,[1,2] Yesid A. Ramirez,[3,4] Tamás Bíró,[5] Jennifer I. Drake,[6] Alison O'Mahony,[6,7] Attila Gábor Szöllősi,[5] Szilárd Póliska,[8] Ana Kilić,[9] Michael Soeberdt,[9,10] Christoph Abels,[9,10] and Attila Oláh[1]

[1]Department of Physiology, Faculty of Medicine, University of Debrecen, Debrecen, Hungary; [2]University of Debrecen, Doctoral School of Molecular Medicine, Debrecen, Hungary; [3]Faculty of Engineering, Design and Applied Sciences. School of Applied Sciences and Sustainable Industry, Department of Pharmaceutical and Chemical Sciences, Universidad Icesi, Cali, Valle del Cauca, Colombia;[4]Cannaflos - Gesellschaft für medizinisches Cannabis mbH., Köln, Germany; [5]Department of Immunology, Faculty of Medicine, University of Debrecen, Debrecen, Hungary; [6]Eurofins Discovery, St. Charles, MO, USA; [7]Recursion, Salt Lake City, UT, USA; [8]Genomic Medicine and Bioinformatics Core Facility, Department of Biochemistry and Molecular Biology, Faculty of Medicine, University of Debrecen, Debrecen, Hungary; [9]Dr. August Wolff GmbH & Co. KG Arzneimittel, Bielefeld, Germany; [10]Bionorica SE, Neumarkt, Germany

Corresponding author:

Dr. habil. Attila Oláh, MD, PhD; Department of Physiology, Faculty of Medicine, University of Debrecen, Nagyerdei krt. 98., H-4032 Debrecen, Hungary; Tel: +3652-255-575; e-mail: olah.attila@med.unideb.hu

SUPPLEMENTARY Methods

Materials

FX (solvent: dimethyl sulfoxide [DMSO]; VWR International, LLC., Radnor, PA, USA) was provided Dr. August Wolff GmbH & Co. KG Arzneimittel (Bielefeld, Germany), whereas the TLR3 activator p(I:C) (Cat. No.: tlrl-picw-250; solvent: endotoxin-free physiological water) and the PI3K-inhibitor GDC0941 (a.k.a. pictilisib; Cat. No.: HY-50094; solvent: DMSO) were purchased from InvivoGen (San Diego, CA, USA) and MedChemExpress LLC (Sollentuna, Sweden), respectively. In every cellular assay, we prepared 1,000× concentrated stock solutions of the materials that have been dissolved in the culture medium in 1:1,000 to achieve the desired working concentrations, and control cultures were always treated by using identical amount of vehicle.

Cell culturing

Primary normal human epidermal keratinocytes (NHEKs) were isolated from dermatologically healthy individuals undergoing surgical interventions following written informed consent adhering to Helsinki guidelines, and after obtaining Institutional Research Ethics Committees and Government Office for Hajdú-Bihar County's permission (document IDs: IX-R-052/01396-2/2012, IF-1647-2/2016, IF-1647-9/2016, IF-778-5/2017, 61566-5/2021/EÜIG, DE RKEB/IKEB 4988-2018). Until the isolation, skin specimens were kept in DMEM (Cat. No. 21068-028; Gibco - Thermo Fisher Scientific, Waltham, MA, USA) supplemented with 1% Pen Strep solution (final concentration of penicillin: 100 IU/ml; final concentration of streptomycin: 100 µg/mL; Cat. No. 15140-122; Gibco - Thermo Fisher Scientific) and Amphotericin B (final concentration: 0.5 µg/mL; Cat. No. 15290-026; Gibco - Thermo Fisher Scientific) for at

least 2 hours at 4°C. Subsequently, 6 mm biopsies of the skin specimens were digested enzymatically in 0.25% trypsin (Cat. No. 27250-018; Gibco - Thermo Fisher Scientific) for 20 hours at 4°C, and the dermo-epidermal border was scraped to obtain cells of the basal layer. Trypsin was deactivated by Green's medium (300 ml DMEM [Cat. No. 31966-021; Gibco - Thermo Fisher Scientific], 150 ml HAM's F12 Nutrient Mix [Cat. No. 21765037; Gibco - Thermo Fisher Scientific], 50 ml FBS [10500-064; Gibco - Thermo Fisher Scientific], 5 ml Pen Strep solution [Cat. No. 15140-122; Gibco - Thermo Fisher Scientific], 5 ml of 4.86 mg/ml adenine [Cat. No. A2786; Sigma-Aldrich, St. Louis, MO, USA], 0.5 ml of 5 mg/ml insulin [Cat. No. I9278; Sigma-Aldrich], 1 ml of 0.2 mg/ml hydrocortisone [Cat. No. H0888; Sigma-Aldrich], 0.5 ml of 1.36 µg/ml triiodothyronine [Cat. No. T2877; Sigma-Aldrich] and 0.5 ml of 10^{-7} M cholera toxin [Cat. No. C8052; Sigma-Aldrich]). Following appropriate washing, the cell suspension was separated from the debris by using a sterile filter (pore size: 100 µm; Cat. No. 22363549; Gibco - Thermo Fisher Scientific). The cell suspension was centrifuged and fresh Green's medium (supplemented with human recombinant epidermal growth factor [0.5 ml of 10 µg/ml; Cat. No. E9644; Sigma-Aldrich]) was added to the cell pellet, and cells were seeded in a density of 50,000 cells/ml to T75 culture dishes in 10 ml supplemented Green's medium (passage 0). Following the attachment of the cells (i.e., ca. on post-isolation days 3-5), culture medium was changed to serum-free EpiLife medium (Cat. No. MEPI500CA; Thermo Fisher Scientific) supplemented with Human Keratinocyte Growth Supplement (Cat. No. S001K; Gibco - Thermo Fisher Scientific) without antibiotics. After this step, culture medium was changed every other day, and the cells were sub-cultured at 60-70% confluence. NHEKs were cultured at 37°C in a 5% CO_2-containing humidified atmosphere, and only keratinocytes below passage

number 4 were used for the experiments. Relevant anamnestic data of the donors can be found in **Table 1**.

Human immortalized HaCaT keratinocytes were cultured in Dulbecco's Modified Eagle Medium (DMEM; Cat. No. 31966-021; Gibco - Thermo Fisher Scientific) supplemented with 10% heat inactivated fetal bovine serum (FBS; Cat. No. 10500-064; Gibco - Thermo Fisher Scientific), and antibiotics (MycoZap™ Plus-CL in 1:500; Cat. No. VZA-2011; Lonza, Basel, Switzerland) at 37°C in a 5% CO_2-containing humidified atmosphere. The medium was changed every other day, and cells were sub-cultured at 70-80% confluence. Cells were regularly checked for *Mycoplasma* contamination by using MycoAlert™ PLUS Mycoplasma Detection Kit (Cat. No. LT07-710; Lonza), and every assessment yielded negative result.

Determination of cellular viability (MTT-assay)

The viability of HaCaT keratinocytes was determined by MTT-assay (Cat. No. M5655-1G; Sigma-Aldrich) measuring the conversion of the tetrazolium salt to formazan by mitochondrial dehydrogenases as described previously (S1). Briefly, cells were plated in 96-well plates (20,000 cells/well), and were treated as indicated. Cells were then incubated with 0.5 mg/ml MTT reagent for 3 hrs, and concentration of formazan crystals (as an indicator of number of viable cells) was determined colorimetrically at 565 nm by using FlexStation 3 multi-mode microplate reader (Molecular Devices, San Francisco, CA, USA). Following appropriate background subtraction, results were expressed as percentage of vehicle control regarded as 100%. Curve fitting and calculation of the highest non-cytotoxic as well as the half-cytotoxic concentration were

performed by using GraphPad Prism 9.3.1 (471) (GraphPad Software, LLC, San Diego, CA, USA).

CyQUANT-assay

The cell count was determined by measuring the DNA content of cells using CyQUANT™ Cell Proliferation Assay Kit (Cat. No. C7026; Thermo Fisher Scientific) as described before (S1). Briefly, HaCaT keratinocytes (5,000 cells per well) were cultured in 96-well “black well/clear bottom” plates (Greiner Bio-One, Frickenhausen, Germany) and were treated as indicated. Supernatants were then removed by blotting on paper towels, and the plates were subsequently frozen at -80°C. The plates were then thawed at room temperature, and 200 µl of CyQUANT dye/cell lysis buffer mixture was added to each well. After 5 min of incubation, fluorescence was measured at 490 nm excitation and 520 nm emission wavelengths using FlexStation 3 multimode microplate reader (Molecular Devices) in well-scan mode (i.e., each well was measured at 9 different locations, and the mean of these measurements was plotted as one data point). Relative fluorescence values were expressed as percentage of vehicle control regarded as 100%.

MitoSOX Red labeling

Mitochondrial production of the reactive oxygen species (mtROS) was monitored by MitoSOX Red superoxide indicator (Cat. No. M36008; Thermo Fisher Scientific). Briefly, HaCaT keratinocytes (20,000 cells per well) were cultured in 96-well “black well/clear bottom” plates (Greiner Bio-One). The cells were loaded by using 5 µM MitoSOX Red superoxide indicator in a serum-free pre-warmed, colorless culture

medium (Sebomed® Basal Medium [Cat. No. F8205; Merck KGaA, Darmstadt, Germany]; 100 µl/well; 10 min; 37°C). The cells were then washed three times by using their usual (for details, see the Methods section of the main text) culture medium (100 µl/well), and were treated as indicated. After 30 min of incubation at 37°C, fluorescence was measured at 510 nm excitation and 580 nm emission wavelengths using FlexStation 3 multimode microplate reader (Molecular Devices) in the aforementioned well-scan mode (i.e., each well was measured at 9 different locations). Following the subtraction of the background signal (measured in unloaded cells on the same plate), the mean of these measurements was plotted as one data point in relative fluorescence units.

Quantitative, real-time polymerase chain reaction (Q-PCR)

Q-PCR was performed on a Roche LightCycler 480 System (Roche, Basel, Switzerland) using the 5' nuclease assay as described before (S1,2). Briefly, total RNA was isolated using TRIzolate reagent (Cat. No. URN0103; UD Genomed, Debrecen, Hungary) or TRI reagent (Cat. No. T9424-200ml; Sigma-Aldrich).

DNase treatment was performed according to the manufacturer's protocol (Ambion DNase I buffer 10× [Cat. No. AM8170G]; Ambion DNase I RNase-free [Cat. No. AM2222]; 0.5M EDTA pH 8.0 [Cat. No. AM9260G] all from Invitrogen - Thermo Fisher Scientific), and then, 1 µg of total RNA was reverse-transcribed into cDNA using High Capacity cDNA Reverse Transcription Kit with RNase Inhibitor (Cat. No. 4374967; Applied Biosystem - Thermo Fisher Scientific).

PCR amplification was performed using the TaqMan® Gene Expression Assays (assay IDs: Hs00174092_m1 for IL-1α, Hs00174097_m1 for IL-1β, Hs00985639_m1 for IL-6,

Hs00174103_m1 for IL-8) and the TaqMan universal PCR master mix protocol (Applied Biosystems). As internal controls, transcripts of 18S ribosomal RNA (RNA 45S5; assay ID: Hs03928985_g1) were determined. The amount of the transcripts was normalized to those of the housekeeping gene using the ΔCT method. Finally, the relative expression values were further normalized to the ones of the vehicle-treated controls (ΔΔCT method).

RNA-Seq method

HaCaT keratinocytes were seeded in 35-mm Petri dishes (500,000 cells/1.5 ml culture medium). The indicated 24-hr treatments (vehicle control, p(I:C) [20 µg/mL], and p(I:C) [20 µg/mL] + FX [14 µM]) were started on the next day using three biological replicates per group. Total RNA was collected as described in the previous section.

To obtain global transcriptome data high throughput mRNA sequencing analysis was performed on Illumina sequencing platform. Total RNA sample quality was checked on Agilent BioAnalyzer using Eukaryotic Total RNA Nano Kit (Cat. No. 5067-1511; Agilent Technologies, Santa Clara, CA, USA) according to manufacturer's protocol. Samples with RNA integrity number (RIN) value >7 were accepted for library preparation process. RNA-Seq libraries were prepared from total RNA using Ultra II RNA Sample Prep kit (Cat. No. E7775S; New England BioLabs; Ipswich, MA, USA) according to the manufacturer's protocol. Briefly, poly-A RNAs were captured by oligo-dT conjugated magnetic beads then the mRNAs were eluted and fragmented at 94°C. First strand cDNA was generated by random priming reverse transcription and after second strand synthesis step double stranded cDNA was generated. After repairing ends, A-tailing and adapter ligation steps adapter ligated fragments were amplified in enrichment PCR

and finally sequencing libraries were generated. Sequencing runs were executed on Illumina NextSeq 500 instrument (Illumina, San Diego, CA, USA) using single-end 75 cycles sequencing.

RNA-Seq data analysis

Raw sequencing data (fastq) was aligned to human reference genome version GRCh38 using HISAT2 algorithm and BAM files were generated. Downstream analysis including principal component analysis (PCA) was performed using StrandNGS software (www.strand-ngs.com). BAM files were imported into the software DESeq algorithm was used for normalization. Moderated T-test was used to determine differentially expressed genes between conditions. PCA was performed by using the normalized gene expression values of all genes. PCA plot represents the relationship of the examined samples to each other. The replicates in the same treatment group show high similarity to each other and the three different treatment groups are clearly separated.

Pathway analysis

Functional enrichment analysis was performed using g:Profiler (version: e109_eg56_p17_1d3191d) with g:SCS multiple testing correction method applying significance threshold of 0.05, using “Ordered query” functionality. The gene lists were uploaded to the g:Profiler web interface, and enrichment analysis was performed against the GO:molecular function pathways database. Said lists contained those genes that were significantly (FC>1.5; $P<0.05$) up- (p(I:C) vs. vehicle control comparison) or down-regulated (p(I:C)+FX vs. p(I:C) comparison) following the

respective treatments, and were ordered by importance in a decreasing manner, where higher fold-change was considered more important.

Raw data of the RNA-Seq analysis are accessible in the NCBI SRA database (hyperlink to the data: http://www.ncbi.nlm.nih.gov/bioproject/1022043).

Cytokine array

Cells were seeded in d=40 mm Petri dishes (0.5 million cells in 1.5 ml culture medium), and were treated as indicated for 3 hours. Supernatants were subsequently collected and centrifuged (500 g for 10 min). Samples were then stored at -80°C before being assayed by Proteome Profiler Human XL Cytokine Array Kit according to the manufacturer's protocol (Cat. No. ARY022B; R&D Systems, Inc., Minneapolis, MN, USA). Briefly, 2 ml of Array Buffer 6 was pipetted into each well of the 4-Well Multi-dish, and the membranes were incubated in this buffer to block non-specific binding sites (1 hour at room temperature on a rocking platform shaker). Next, Array Buffer 6 was removed, and the membranes were incubated with 1.5 ml of the supernatants overnight at 4°C on a rocking platform shaker. Subsequently, the membranes were washed three times in 20 ml Wash buffer (3×10 minutes at room temperature), and were then incubated with 1.5 ml diluted Detection Antibody Cocktail (1 hour at room temperature). Following appropriate washing, 1× Streptavidin-HRP was added to the membranes that were subsequently incubated for 30 minutes at room temperature. Finally, following the last washing steps, the immunoreactive spots were visualized by Chemi Reagent Mix using a Kodak Gel Logic 1500 Imaging System (Kodak, Tokyo, Japan).

Semi-quantitative densitometric analysis of the signals was performed using the freely available *ImageJ 1.49v* software (National Institute of Health, Bethesda, MD, USA). Briefly, means of the negative control spots on each membrane were considered as background signal intensities, and were subtracted from the raw values. Means of the two technical repeats available on the membranes for each molecule were then normalized to the respective control data, and ≥1.5-fold alteration upon p(I:C)-treatment was considered to be relevant alteration (**Supplementary Table S1**).

ELISA (IL-6, IL-8, endothelin)

Cells were seeded in d=40 mm Petri dishes (0.5 million cells in 1.5 ml culture medium), and were treated as indicated. Supernatants were subsequently collected and centrifuged (500 g for 10 min). Samples were then stored at -80°C before being assayed by OptEIA™ Set Human ELISA Kits for IL-6 and IL-8 (Cat. No.-s 555220 and 555244, respectively; BD Biosciences, Franklin Lakes, NJ, USA) and Endothelin Pan Specific DuoSet ELISA Kit (Cat. No. DY1160; R&D Systems, Inc.) following the manufacturers' protocol.

Western blot analysis

Four different passages of HaCaT keratinocytes were seeded in 90-mm Petri dishes (1,000,000 cells/6 ml culture medium), and the indicated 60-min treatments were executed on the next day. Cells were then harvested in lysis buffer (50 mM Tris-HCl, pH 7.5 [Cat. No. 28811.285; VWR International, LLC., Radnor, PA, USA], 150 mM NaCl [Cat. No. 27800.291; VWR International], 1 (V/V)% Triton™ X-100 [Cat. No. X100-500ML; Sigma-Aldrich, St. Louis, MO, USA], 1 (V/V)% IGEPAL® CA-630 [Cat.

No. I3021-50ML; Sigma-Aldrich], sodium deoxycholate [500 mg in 100 ml; Cat. No. D6750-100G; Sigma-Aldrich] in distilled water) that contained protease inhibitor cocktail (dilution: 1:100; Cat. No. P8340-5 ml; Sigma-Aldrich), and PhosSTOP (1 tablet/10 ml; [Cat. No. 4906837001; Roche, Basel, Switzerland]), and the protein content was measured by a modified BCA protein assay (Cat. No. 1859078; Pierce, Rockford, IL, USA). The samples were then subjected to sodium dodecyl sulfate-polyacrylamide gel electrophoresis. 10% Mini Protean TGX gels (Cat. No. 4561033; Bio-Rad, Hercules, CA, USA) were loaded with equal (15 µg) amount of protein per lane. Samples were then transferred to nitrocellulose membranes, by using Trans-Blot Turbo Midi 0.2 µm Nitrocellulose Transfer Pack (Cat. No. 1704159; Bio-Rad) and Trans-Blot Turbo™ System (Bio-Rad). The membranes were then probed overnight at 4°C with mouse-anti-human p-IκBα specific primary antibodies (Cat. No. 9246L; Cell Signaling Technology, Danvers, Massachusetts, USA) applied in 1:1,000 dilution in 1% milk containing TBST (50 mM Tris, 0.1 (V/V)% TWEEN® 20 [Cat. No. P7949; Sigma-Aldrich], 150 mM NaCl [Cat. No. 27800.291; VWR International] pH 7.5), or with mouse-anti-human diphosphorylated p38 MAP kinase specific primary antibodies (Cat. No.: M8177; Sigma-Aldrich; 1:2,000 dilution in 1% milk containing TBST). As secondary antibody, a horseradish peroxidase-conjugated, goat-anti-mouse IgG Fc segment-specific antibody (Cat. No.: 170-6516; Bio-Rad; 1:5,000 dilution in 1% milk containing TBST; at room temperature, for 1 hour) was used, and the immunoreactive bands were visualized by SuperSignal™ West Pico PLUS Chemiluminescent Substrate enhanced chemiluminescence kit (Cat. No. 34580; Thermo Fisher Scientific, Waltham, MA, USA) or SuperSignal™ West Femto Maximum Sensitivity Substrate (Cat. No. 34096; Thermo Fisher Scientific) using a KODAK Gel Logic 1500 Imaging System (Eastman Kodak Company, Kodak, Tokyo, Japan). To assess equal loading,

antibodies were stripped by using 0.2 N NaOH (Cat. No. 06203-1KG; Sigma-Aldrich) and the membranes were re-probed with rabbit-anti-β-tubulin antibodies (Cat. No. ab6046; Abcam, Cambridge, UK; or Cat. No. NB600-93655; Novus Biologicals, Englewood, Colorado, USA; 1:1,000 dilution in 1% milk and BSA containing TBST at 4°C overnight), and visualized as described above using a horseradish peroxidase-conjugated goat-anti-rabbit IgG Fc-segment-specific secondary antibody (1:10,000 in 1% milk containing TBST; Cat. No. 170-6516; Thermo Fisher Scientific; at room temperature, for 1 hour). Semi-quantitative densitometry analysis of the signals was performed by using *ImageJ 1.52a software* (National Institutes of Health, Bethesda, MD, USA).

BioMAP® Diversity PLUS® profile analysis

The BioMAP® Diversity PLUS® panel of 12 human primary cell-based systems are designed by Eurofins Discovery (St. Charles, MO, USA) to model complex human tissue and disease biology of the vasculature, skin, lung, and inflammatory tissue in an *in vitro* format. It is a standard panel that has been continuously running as a commercial service for more than 10 years. Detailed description of the method can be found in our previous publications.[55-57] BioMAP technology is covered by patents US10018621B2, US9734282B2, US8697387B2, US8467970B2, US8019551B2, US7912651B2, US7908089B2, US7266458B2, US6763307B2, and US6656695B2.

Cell Culture

BioMAP systems were plated as described previously.[55-57] Each system is a combination of one or more human primary cells, a stimulus, and a set of biomarker

readouts (**Supplementary Table S2**). FX was prepared in DMSO (final concentration < 0.1%) and tested at concentrations of 14 µM, 4.7 µM, 1.6 µM, and 520 nM.

Data Analysis

Test agent-treated sample biomarker measurements are divided by the average of control samples (n > 6 vehicle controls from the same plate) to generate a ratio. The ratio of test agent to vehicle control is $\log_{10}$ transformed. The significance envelope is calculated using historical vehicle control data at a 95% confidence interval.

Profile Analysis

Profile Analysis Biomarker activities are annotated when two or more consecutive concentrations charge in the same direction relative to vehicle controls, are outside of the significance envelope, and have at least one concentration with an effect size > 20% ($|\log_{10} ratio| > 0.1$). Annotated biomarker activities are described as modulated if they increase in some systems, but decrease in others. Cytotoxicity is noted when total protein levels decrease by more than 50% (log10 ratio of sulforhodamine B [SRB; adherent cells] or Alamar Blue [non-adherent cells] levels < -0.3) and are indicated by a thin black arrow above the X-axis. Anti-proliferative effects are defined by an SRB (adherent cells) or Alamar Blue (non-adherent cells) $\log_{10}$ *ratio* value < -0.1 from cells plated at a sub-confluent level and are indicated by gray arrows above the X-axis. Cytotoxic and anti-proliferative effects require only one concentration to meet the indicated threshold for profile annotation.

Z-score calculation

To determine the extent of similarity between BioMAP profiles of compounds run in the Diversity PLUS Panel, a custom similarity metric (BioMAP Z-Standard) has been developed that is a combinatorial approach that has improved performance in

mechanism classification of reference agents compared to other measures tested (including Pearson's and Spearman's correlation coefficients). This approach more effectively accounts for variations in the number of data points, systems, active biomarker readouts and the amplitude of biomarker readout changes that are characteristic features of BioMAP profiles. A Pearson's correlation coefficient (*r*) is first generated to measure the linear association between two profiles that is based on the similarity in the direction and magnitude of the relationship. Since the Pearson's correlation can be influenced by the magnitude of any biomarker activity, a per-system weighted average Tanimoto metric is used as a filter to account for underrepresentation of less robust systems. The Tanimoto metric does not consider the amplitude of biomarker activity, but addresses whether the identity and number of readouts are in common on a weighted, per system basis. A real-value Tanimoto metric is calculated first by normalizing each profile to the unit vector (e.g., $A = \frac{A}{\| A \|}$) and then applying the following formula: $\frac{A \cdot B}{\| A \| + \| B \| - A \cdot |B}$,

where A and B are the two profile vectors. Then, it is incorporated into a system weighted-averaged real-value Tanimoto metric in this calculation: = $\frac{\sum Wi \cdot Ti}{\sum Wi}$. The calculation uses the real-value Tanimoto score for each *i*th system (T_i) and the weight of each *i*th system (W_i). W_i is calculated for each system in the following formula: $\frac{1}{1+e^{-100*(lr-0.09)}}$, where lr is the largest absolute value of the ratios from the two profiles being compared. Based on the optimal performance of reference compounds, profiles are identified as having mechanistically relevant similarity if the Pearson's correlation coefficient (*r*) ≥ 0.7.[57] Finally, a Fisher *r*-to-z-transformation is used to calculate a z-score to convert a short tail distribution into a normal distribution as follows: $z = 0.5 \log_{10} \frac{1+r}{1-r}$. Then the BioMAP Z-Standard, which adjusts for the number of common

readouts (CR), is generated according to the following formula: Z-Standard = $z = \sqrt{CR - 3}$. A larger BioMAP Z-Standard value corresponds to a higher confidence level, and this is the metric used to rank similarity results.

Molecular docking

The crystal structure of the GDC0941-PI3K complex (PDB ID: 3DBS) was retrieved from the Protein Data Bank (PDB) (S3). Removal of ligands and water molecules was performed using PyMOL version 1.7.5.0 (S4). Kollman charges and polar hydrogens were added by default as set by AutoDockTools (ADT) within MGLTools 1.5.7 (S5). Pose reproduction performance was assessed by root-mean-square deviation (RMSD) between docked poses and the experimental binding pose of GDC0941. The 3D structure file for FX was downloaded from the PubChem Compound Database of the National Biotechnology Information Center of the United States (S6). Gasteiger charges were computed by default, and all torsions were allowed to rotate. Geometry optimization for all ligands was performed using the MMFF94x (S7,8) force field. Grid maps were generated using Autogrid 4.2 with a grid box size of 50 × 50 × 50 and default spacing of 0.375 Å. The grid center (X, Y, Z) for GDC0941 and FX was 23.006, 62.976 and 21.682. AutoDock 4.24 was used to dock the ligands (GA runs: 50; Population Size: 300; maximum Number of evaluations: 2,500,000; Maximum Number of Generations: 27,000). The rest of the Genetic Algorithm Parameters (GA) were set by default. The 50 best scored poses were ranked by binding energy and visually inspected using PyMOL version 1.7.5.0 (S4). All simulations were performed on an ASUS GL502V workstation.

Assessment of PI3K-activity

Activity of PI3K was determined by using PI3K-Glo™ Class I Profiling Kit (a cell-free enzyme activity assay kit; Cat. No. V1690; Promega, Madison, WI, USA), following the manufacturer's instructions. Briefly, we tested the inhibitory efficiency of FX in 96-well plate format using 330 ng/ml kinase (p110δ/p85α) in a final reaction volume of 100 µl/well. The optimal enzyme concentration (resulting in ca. 5% conversion rate) was determined in multiple preliminary experiments (data not shown). DMSO content was kept 2.5% in all cases. Luminescence was determined by using FlexStation 3 multi-mode microplate reader (Molecular Devices) in well-scan mode with nine intra-well repeats, or (in case of some of the preliminary experiments) Envision® 2105 Multimode Plate Reader (PerkinElmer, Waltham, MA, USA). Following appropriate background subtraction, results were expressed as percentage of vehicle control regarded as 100%. Outliers were identified by the ROUT method (Q=10%; GraphPad Prism 9.3.1 (471); GraphPad Software).

Statistical analysis

Data were analyzed by GraphPad Prism 9.3.1 (471) (GraphPad Software). Depending on the sample size, Gaussian distribution was tested by Anderson-Darling or Shapiro-Wilk tests. In case of Gaussian distribution, Student's two-tailed, unpaired t-test (paired comparisons), one-way ANOVA followed by Šídák's multiple comparisons test (multiple comparisons) or Dunnett's multiple comparisons test (comparison to a single control group) were used, whereas in case of non-Gaussian distribution, two-tailed Mann-Whitney test (paired comparisons) or Kruskal-Wallis test followed by Dunn's multiple comparisons test (multiple comparisons) were used, and $P<0.05$ values were

regarded as significant differences. Graphs were plotted using GraphPad Prism 9.3.1 (471).

SUPPLEMENTARY DISCUSSION

Keratinocytes and beyond: Anti-inflammatory and endothelin-suppressing actions of FX at a greater perspective

It is also noteworthy that suppression of endothelin release may be beneficial in several other diseases and pathological conditions. Indeed, without being exhaustive, endothelin 1 serum level was found to be elevated, and is thought to contribute to the pathogenesis of pulmonary hypertension (S9), alcohol-associated liver disease (S10), systemic sclerosis (S11), endothelial dysfunction and systemic hypertension (S12), as well as preeclampsia and preeclampsia-associated podocytopathy (S13,14). Likewise, pharmacological blockade of the actions of endothelin 1 may be beneficial in the treatment of certain tumors (S15), as well as in preventing vein graft occlusion after coronary artery bypass surgery (S16), and in abrogating aneurysmal subarachnoid hemorrhage-induced cerebral vasospasm (S17). Thus, our data shall encourage one to systematically explore, whether the observed FX-mediated suppression of endothelin release reflects a general, cell type-independent action, because if this were the case, FX could theoretically exert beneficial effects in the above diseases.

Last, but not least, it should also be noted that administration of FX was recently shown to beneficially influence the clinical outcome in COVID-19 patients.[33-35] Although it would be premature to draw bold conclusions, it is worth mentioning that according to our cytokine array data, FX appears to shape the immunological response of epidermal keratinocytes in a way that may be desirable in SARS-CoV-2 infection (for details, see **Supplementary Table S1**). Considering that pharmacological inhibition of the PI3K pathway has been suggested being beneficial in SARS-CoV-2 infection (S18-20), one might speculate that the recently reported beneficial effects of FX in COVID-19

patients[33,35] might have been (at least in part) the consequence of FX-mediated interference with the PI3K-pathway.

SUPPLEMENTARY FIGURES

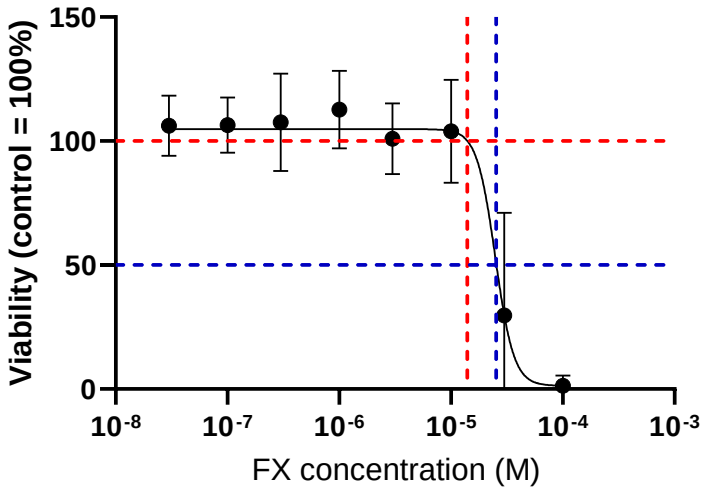

Supplementary Figure S1 *FX concentration-dependently decreases viability of HaCaT keratinocytes in course of 24-hr treatments*

A) MTT-assay. HaCaT keratinocytes were treated using various concentrations of FX (or vehicle) for 24 hours. Background signal intensity was subtracted, and then data are presented following their normalization to the mean of the vehicle-treated control group (regarded as 100%) as mean±SD of N=12 biological replicates. Dashed blue lines indicate half-cytotoxic concentration (i.e., the concentration at which calculated MTT signal intensity decreased to 50% of the vehicle-treated control; ~25.43 μM). Dashed red lines indicate 14 μM, i.e., the highest concentration at which calculated MTT signal intensity did not decrease below the level of the vehicle-treated control group (100%). **FX:** fluoxetine.

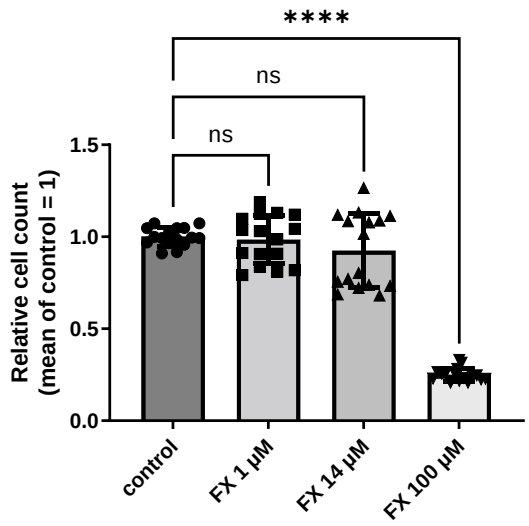

Supplementary Figure S2 *Up to 14 µM, FX does not decrease the cell count of HaCaT keratinocytes over the course of 24-hr treatments, whereas it exerts cytotoxic effects at 100 µM*

CyQUANT-assay. Data are presented following their normalization to the mean of the vehicle-treated control group (regarded as 1) as mean±SD of N=16 biological replicates. ****P<0.0001 as indicated. **ns:** not significant. **FX:** fluoxetine.

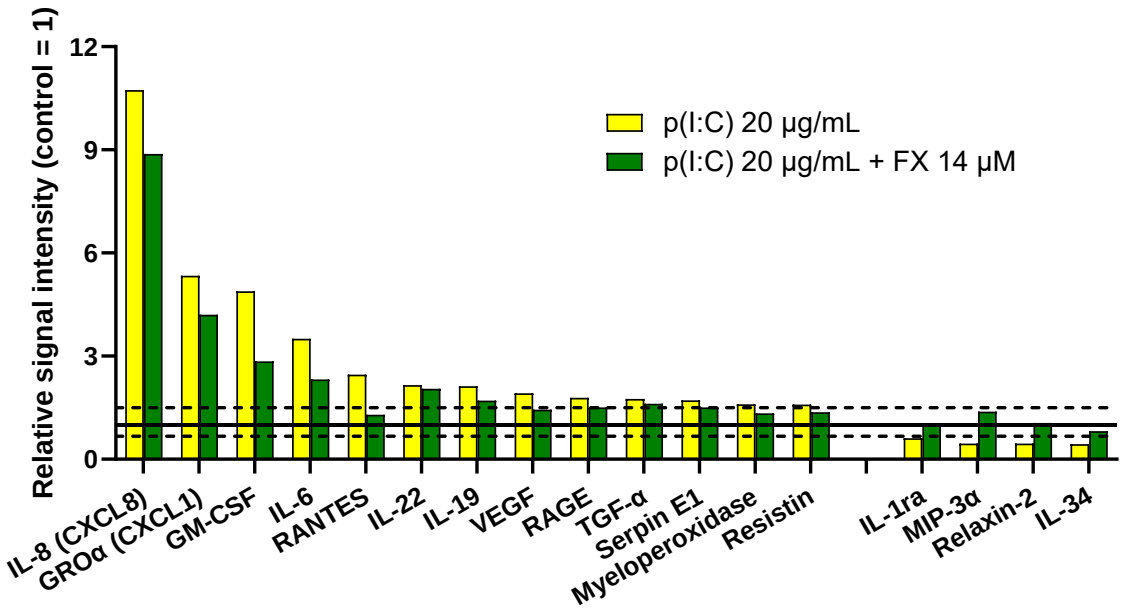

Supplementary Figure S3 *FX appears to suppress the pro-inflammatory effects of p(I:C) in HaCaT keratinocytes following 3-hr treatments*

HaCaT keratinocytes were treated as indicated for 3 hours. Supernatants were collected and subsequently assayed by using a cytokine array kit. Following appropriate background subtraction, mean signal intensities (calculated from data of 2 technical replicates) were normalized to the mean signal intensity of the same molecule measured in case of the vehicle-treated control culture (control = 1; solid line). ≥1.5-fold p(I:C)-induced increase or decrease of the signal intensity was considered as relevant alteration (indicated by dashed lines). **FX:** fluoxetine; **GM-CSF:** granulocyte-macrophage colony-stimulating factor, a.k.a. colony-stimulating factor 2; **GROα:** C-X-C motif chemokine ligand 1; **IL:** interleukin; **IL-1ra:** interleukin 1 receptor antagonist; **MIP-3α:** C-C motif chemokine ligand 20; **p(I:C):** polyinosinic-polycytidylic acid; **RAGE:** advanced glycosylation end-product specific receptor; **RANTES:** C-C motif chemokine ligand 5; **TGF:** transforming growth factor; **VEGF**: vascular endothelial growth factor A.

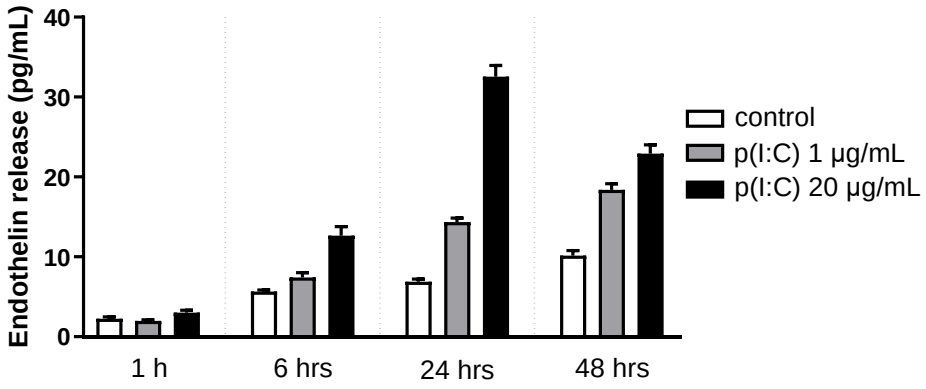

Supplementary Figure S4 *p(I:C) concentration- and time-dependently increases endothelin-release from human epidermal keratinocytes*

HaCaT keratinocytes were treated as indicated for 1, 6, 24, or 48 hours. Supernatants were collected and subsequently assayed by using a pan-endothelin ELISA kit to detect endothelin release. Data are expressed as mean±SD of 3 technical replicates. **p(I:C):** polyinosinic-polycytidylic acid (20 µg/mL).

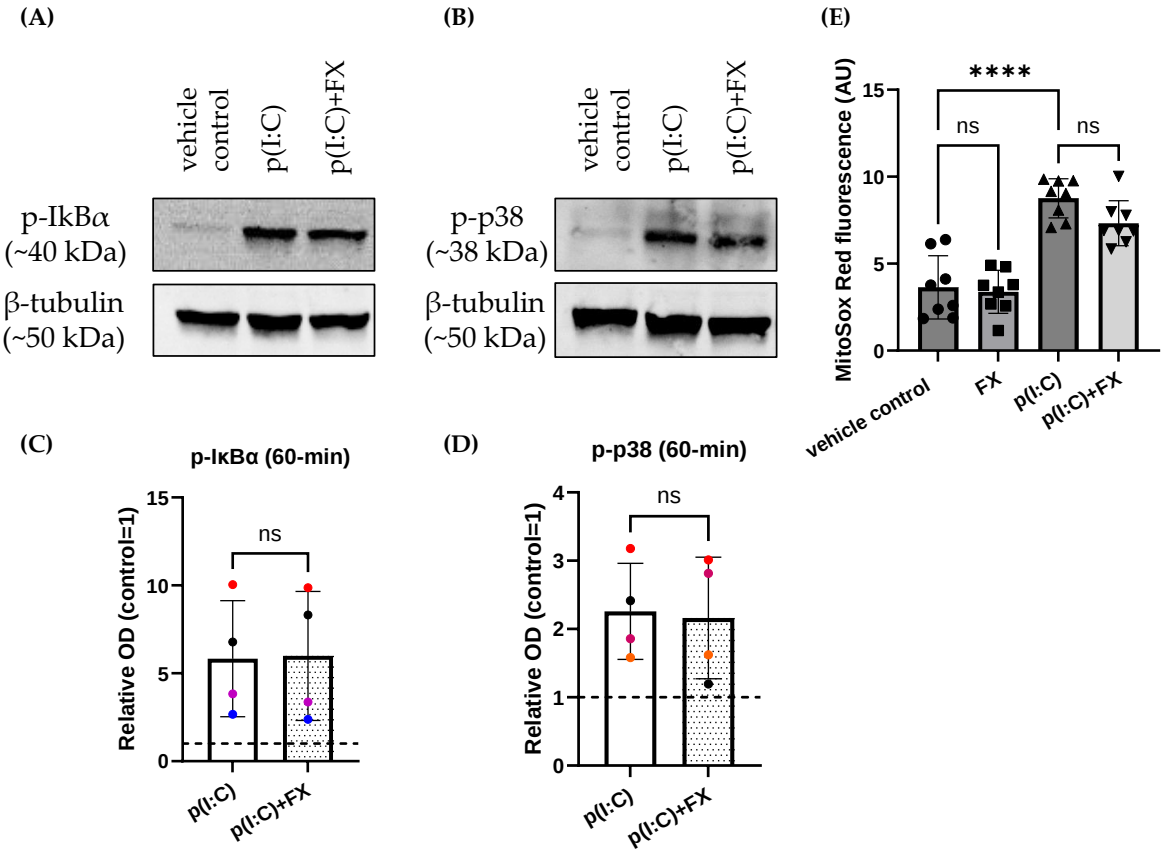

Supplementary Figure S5 *FX does not interfere with the NF-κB and p38 MAPK pathways, and fails to significantly suppress p(I:C)-induced mitochondrial reactive oxygen species (mtROS) production.*

(**A-B**) Western blots. Four different passages of HaCaT keratinocytes were treated as indicated for 60 min, and were then harvested to perform western blot analysis. Panel **A** and **C** show representative immunoblots of p-IκBα (**A**) and for p-p38 (**B**), while results of the densitometry analysis are shown on panels **C** and **D**. Mean of the vehicle-treated control cultures is shown as a dashed line. Data are expressed as mean±SD of 4 biological replicates. Each color represents data from an independent passage. (**E**) Assessment of mitochondrial ROS production by MitoSOX Red labeling following the indicated, 30-min treatments. Data are expressed as mean±SD of 8 biological replicates. ****P<0.0001. **FX:** fluoxetine (14 μM); **ns:** not significant; **p(I:C):** polyinosinic-polycytidylic acid (20 μg/mL).

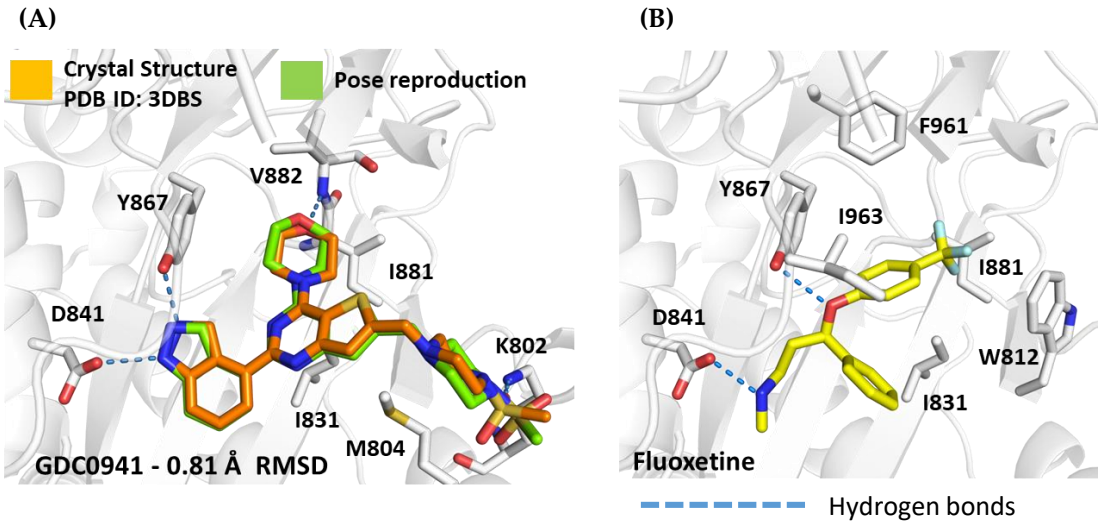

Supplementary Figure S6 *GDC0941 and FX may occupy the same binding site on PI3K*

A) Pose reproduction of GDC0941 (0.81 Å RMSD). (**B**) Top scored AutoDock pose for Fluoxetine within the ATP binding site of PI3K gamma subunit. Hydrogen bonds are denoted with blue dashed lines.

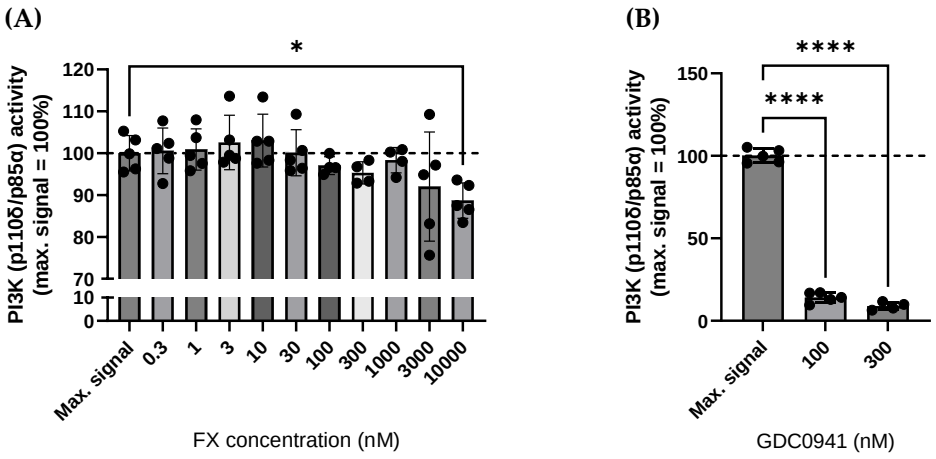

Supplementary Figure S7 *FX is a weak inhibitor of PI3K*

A-B: PI3K-activity assay. FX exerts minor inhibition on PI3K activity in a cell-free enzyme activity assay. Data are expressed as mean±SD of N=4-5 replicates (each determined as mean of nine intra-well technical replicates), as indicated. Mean of the vehicle (DMSO)-treated control group is shown as a dashed line. *P<0.05, and ****P<0.0001, respectively, as indicated. **FX:** fluoxetine.

SUPPLEMENTARY TABLES

Supplementary Table S1 *List of those molecules that exhibited relevant (≥1.5-fold) alterations on the cytokine array following 3-hr treatments with 20 μg/mL p(I:C).*

Abbreviation	Full name	FC over control upon p(I:C)-treatment	FC over control upon p(I:C)+FX-treatment	Notes (unless indicated otherwise, the source of the information was https://www.ncbi.nlm.nih.gov/gene; accessed on: 01/27/2022)
IL-8	Interleukin 8 (a.k.a. C-X-C motif chemokine ligand 8)	10.74165865	8.878189582	It functions as a chemotactic factor by guiding the neutrophils to the site of infection. Bacterial and viral products rapidly induce IL-8 expression. IL-8 also participates with other cytokines in the proinflammatory signaling cascade and plays a role in systemic inflammatory response syndrome (SIRS). Its higher levels correlate with worse prognosis in COVID-19 (S21).
GROα	C-X-C motif chemokine ligand 1	5.341499561	4.202264249	Neutrophil chemoattractant. Aberrant expression of this protein is associated with the growth and progression of certain tumors. Its level increases in severe/critical COVID-19 patients (S22).
GM-CSF	Colony stimulating factor 2	4.885446879	2.849885683	A cytokine that controls the production, differentiation, and function of granulocytes and macrophages. Elevated levels of GM-CSF have been detected in SARS-CoV-2 infected patients that develop acute respiratory distress syndrome.
IL-6	Interleukin 6	3.505016084	2.325846593	A cytokine that functions in inflammation and helps the maturation of B cells. Elevated levels of IL-6 have been found in COVID-19.
RANTES	C-C motif chemokine ligand 5	2.457841369	1.297757141	Chemoattractant for blood monocytes, memory T helper cells and eosinophils. High SARS-CoV-2 viral load and low CCL5 expression levels were associated with intensive care unit admission or death (S23).
IL-22	Interleukin 22	2.158444906	2.052078213	A member of the IL-10 cytokine family. IL-22 is a crucial in regulating host immunity in COVID-19.
IL-19	Interleukin 19	2.12245083	1.703904209	Member of the IL-10 cytokine family. It up-regulates the SARS-CoV-2 entry receptor ACE2 expression in the airway epithelium (S24).
VEGF	Vascular endothelial growth factor A	1.919266193	1.44037364	This growth factor induces proliferation and migration of vascular endothelial cells, and is essential for both physiological and pathological angiogenesis. The levels of VEGF are increased during SARS-CoV-2 infection, thus promoting inflammation by facilitating recruitment of inflammatory cells, and by increasing the level of angiopoietin II, one of two products of the SARS-CoV-2 binding target, angiotensin-converting enzyme 2 (ACE2). In turn, angiopoietin II facilitates the elevation of

				VEGF, thus forming a vicious cycle in the release of inflammatory cytokines.
RAGE	Advanced glycosylation end-product specific receptor	1.788664054	1.51229135	Impairing RAGE signaling promotes survival and limits disease pathogenesis following SARS-CoV-2 infection in mice (S25).
TGF-α	Transforming growth factor alpha	1.752131272	1.613493182	A growth factor that is a ligand for the epidermal growth factor receptor, which activates a signaling pathway for cell proliferation, differentiation and development.
Serpin E1	Serpin family E member 1 (Plasminogen Activator Inhibitor 1)	1.716273213	1.508567524	A member of the serine proteinase inhibitor (serpin) superfamily. It is a hair growth promoting adipokine (S26). Plasminogen activator inhibitor-1 level was elevated in patients with severe COVID-19; hypercoagulability in COVID-19 may be because of decreased fibrinolysis resulting from inhibition of plasmin through high levels of plasminogen activator inhibitor-1 (S27).
	Myeloperoxidase	1.598750074	1.338496749	This enzyme produces hypohalous acids central to the microbicidal activity of neutrophils.
	Resistin	1.589266474	1.365840924	Resistin has an antimicrobial role in skin, displaying antibacterial activity against both Gram-positive and Gram-negative bacteria. Its higher levels correlate with worse prognosis in COVID-19 (S21).
IL-1ra	Interleukin 1 receptor antagonist	0.614673757	0.994571594	It inhibits the activities of IL-1α and IL-1β, and modulates a variety of IL-1-related immune and inflammatory responses, particularly in the acute phase of infection and inflammation. Its higher levels correlate with worse prognosis in COVID-19 (S21).
MIP-3α	C-C motif chemokine ligand 20 (CCL20)	0.458883529	1.387978784	It displays chemotactic activity for lymphocytes, and can repress proliferation of myeloid progenitors. Patients suffering from severe COVID-19 pneumonia displayed significantly increased plasma levels of CCL20 (S28).
	Relaxin 2	0.458724987	1.052353792	It exerts anti-fibrotic effects in systemic sclerosis (S29). SARS-CoV-2 can disturb relaxin signaling (S30).
IL-34	Interleukin 34	0.440558007	0.818161215	It promotes the differentiation and viability of monocytes and macrophages through the colony-stimulating factor-1 receptor. IL-34 level was found to be lower in SARS-CoV-2 infected peripheral blood mononuclear cell containing human reconstituted organotypic airway epithelium as compared to the noninfected control (S31).

*Potentially SARS-CoV-2-relevant data are highlighted by green (potentially desired effects exerted by FX) or yellow (potentially detrimental effects exerted by FX) background.

Supplementary Table S2 *Overview of the model systems used for BioMAP® Diversity PLUS® panel*

System	Primary Human Cell Type(s)	Stimulation	Disease Relevance	Biomarker Readouts
3C	Venular endothelial cells	IL-1β, TNFα, IFNγ	Chronic Inflammation Cardiovascular Disease	MCP-1, VCAM-1, TM, TF, ICAM-1, E-selectin, uPAR, IL-8 (CXCL8), MIG, HLA-DR, Proliferation, SRB
4H	Venular endothelial cells	IL-4 and histamine	Asthma, Allergy, Autoimmunity	MCP-1, Eotaxin-3, VCAM-1, P-selectin, uPAR, SRB, VEGFR2
LPS	Venular endothelial cells, Peripheral blood mononuclear cells	TLR4 ligand	Chronic Inflammation Cardiovascular Disease	MCP-1, VCAM-1, TM, TF, CD40, E-selectin, CD69, IL-8 (CXCL8), IL-1α, M-CSF, $sPGE_2$, SRB, sTNFα
SAg	Venular endothelial cells, Peripheral blood mononuclear cells	TCR ligands (1×)	Chronic Inflammation, Autoimmune Disease	MCP-1, CD38, CD40, E-selectin, CD69, IL-8 (CXCL8), MIG, PBMC Cytotoxicity, Proliferation, SRB
BT	B cells, Peripheral blood mononuclear cells	α-IgM and TCR ligands (0.001×)	Asthma, Allergy, Oncology, Autoimmunity	B cell Proliferation, PBMC Cytotoxicity, Secreted IgG, sIL-17A, sIL-17F, sIL-2, sIL-6, sTNFα
BF4T	Bronchial epithelial cells, Dermal fibroblasts	TNFα and IL-4	Asthma, Allergy, Fibrosis, Lung Inflammation	MCP-1, Eotaxin-3, VCAM-1, ICAM-1, CD90, IL-8 (CXCL8), IL-1α, Keratin 8/18, MMP-1, MMP-3, MMP-9, PAI-1, SRB, tPA, uPA
BE3C	Bronchial epithelial cells	IL-1β, TNFα, IFNγ	Lung Inflammation, COPD	ICAM-1, uPAR, IP-10, I-TAC, IL-8 (CXCL8), MIG, EGFR, HLA-DR, IL-1α, Keratin 8/18, MMP-1, MMP-9, PAI-1, SRB, tPA, uPA
CASM3C	Coronary artery smooth muscle cells	IL-1β, TNFα, IFNγ	Cardiovascular Inflammation, Restenosis	MCP-1, VCAM-1, TM, TF, uPAR, IL-8 (CXCL8), MIG, HLA-DR, IL-6, LDLR, M-CSF, PAI-1, Proliferation, SAA, SRB
HDF3CGF	Dermal fibroblasts	IL-1β, TNFα, IFNγ, EGF, bFGF, PDGF-BB	Fibrosis, Chronic Inflammation	MCP-1, VCAM-1, ICAM-1, Collagen I, Collagen III, IP-10, I-TAC, IL-8 (CXCL8), MIG, EGFR, M-CSF, MMP-1, PAI-1, Proliferation_72hr, SRB, TIMP-1, TIMP-2
KF3CT	Keratinocytes, Dermal fibroblasts	IL-1β, TNFα, IFNγ, TGFβ	Psoriasis, Dermatitis, Skin Biology	MCP-1, ICAM-1, IP-10, IL-8 (CXCL8), MIG, IL-

				1α, MMP-9, PAI-1, SRB, TIMP-2, uPA
MyoF	Lung fibroblasts	TNFα, TGFβ	Fibrosis, Chronic Inflammation, Wound Healing, Matrix Remodeling	αSM Actin, bFGF, VCAM-1, Collagen I, Collagen III, Collagen IV, IL-8 (CXCL8), Decorin, MMP-1, PAI-1, TIMP-1, SRB
lMphg	Venular endothelial cells, Macrophages	TLR2 ligand	Cardiovascular Inflammation, Restenosis, Chronic Inflammation	MCP-1, MIP-1α, VCAM-1, CD40, E-selectin, CD69, IL-8 (CXCL8), IL-1α, M-CSF, sIL-10, SRB, SRB-Mphg

List of abbreviations. **bFGF:** basic fibroblast growth factor; **CD:** cluster of differentiation; **EGF:** epidermal growth factor; **EGFR:** epidermal growth factor receptor; **HLA-DR:** class II histocompatibility antigen; **ICAM-1:** intercellular Adhesion Molecule 1; **IFNγ:** interferon gamma; **IL:** interleukin; **IP-10:** Interferon gamma-induced protein 10; **I-TAC:** interferon–inducible T cell alpha chemoattractant; **LDLR:** low density lipoprotein receptor; **MCP-1:** monocyte chemoattractant protein-1; **M-CSF:** macrophage colony-stimulating factor; **MIG:** monokine induced by interferon gamma; **MIP-1α:** macrophage inflammatory protein-1, alpha; **MMP:** matrix metalloproteinase; **PAI-1:** plasminogen activator inhibitor-1; **PDGF-BB:** platelet derived growth factor BB; **PBMC Cytotoxicity:** peripheral blood mononuclear cell cytotoxicity; **Proliferation_72hr:** proliferation measured at 72 hours; **SAA:** serum amyloid A; **Secreted IgG:** secreted immunoglobulin G; **sIL:** soluble interleukin; **sPGE2:** soluble prostaglandin E_2; **SRB:** sulforhodamine B; **SRB-Mphg:** sulforhodamine B measured on macrophage only; **sTNFα:** soluble tumor necrosis factor, alpha; **TCR:** T-cell receptor; **TF:** tissue factor; **TGFβ:** transforming growth factor beta; **TIMP:** tissue inhibitor of metalloproteinases; **TLR:** toll-like receptor; **TM:** thrombomodulin; **TNFα:** tumor necrosis factor, alpha; **tPA:** tissue plasminogen activator; **uPA:** urokinase-type plasminogen activator; **uPAR:** urokinase plasminogen activator surface receptor; **VCAM-1:** vascular cell adhesion molecule 1; **VEGFR2:** vascular endothelial growth factor receptor 2; **α-IgM:** alpha immunoglobulin M; **αSM Actin:** alpha smooth muscle actin.

Supplementary Table S3 *Scores of the top five AutoDock poses for GDC0941 (redocking) and FX with corresponding RMSD clustering data. Poses shown in* ***Supplementary Figure S6*** *are highlighted in bold*

Test agent	Rank	Binding Energy (kcal/mol)	Cluster RMSD (Å)	Poses in cluster*	Total clusters**
GDC0941	**1**	**-10.62**	**0.00**	26	4
	2	-10.62	0.36		
	3	-10.61	0.07		
	4	-10.57	0.42		
	5	-10.53	0.24		
FX	**1**	**-8.05**	**0.00**	29	4
	2	-8.01	0.39		
	3	-8.01	0.62		
	4	-7.97	0.49		
	5	-7.85	1.14		

*Out of 50 poses. **2.0 Å root-mean-square deviation (RMSD) tolerance.

FX: fluoxetine.

SUPPLEMENTARY REFERENCES

S1. Markovics A, Angyal Á, Tóth KF, et al. GPR119 Is a Potent Regulator of Human Sebocyte Biology. J Invest Dermatol. 2020;140(10):1909-1918.e8. doi:10.1016/j.jid.2020.02.011

S2. Markovics A, Tóth KF, Sós KE, et al. Nicotinic acid suppresses sebaceous lipogenesis of human sebocytes via activating hydroxycarboxylic acid receptor 2 (HCA2). J Cell Mol Med. 2019;23(9):6203-6214. doi:10.1111/jcmm.14505

S3. Berman HM, Westbrook J, Feng Z, et al. The Protein Data Bank. Nucleic Acids Res. 2000;28(1):235-242. doi:10.1093/nar/28.1.235

S4. PyMOL | pymol.org [Internet]. [cited 2022 Mar 27] DOI: https://pymol.org/2/

S5. Sanner MF. Python: a programming language for software integration and development. J Mol Graph Model. 1999;17(1):57-61.

S6. Kim S, Chen J, Cheng T, et al. PubChem in 2021: new data content and improved web interfaces. Nucleic Acids Res. 2021;49(D1):D1388-D1395. doi:10.1093/nar/gkaa971

S7. Halgren TA. Merck molecular force field. I. Basis, form, scope, parameterization, and performance of MMFF94. Journal of Computational Chemistry. 1996;17(5-6):490-519. doi:10.1002/(SICI)1096-987X(199604)17:5/6<490::AID-JCC1>3.0.CO;2-P

S8. Halgren TA. MMFF VII. Characterization of MMFF94, MMFF94s, and other widely available force fields for conformational energies and for intermolecular-interaction energies and geometries. J Comput Chem. 1999;20(7):730-748. doi:10.1002/(SICI)1096-987X(199905)20:7<730::AID-JCC8>3.0.CO;2-T

S9. Cansu DÜ, Korkmaz C. Pulmonary hypertension in connective tissue diseases: epidemiology, pathogenesis, and treatment. Clin Rheumatol. Published online 2022. doi:10.1007/s10067-022-06446-y

S10. Chen J, Argemi J, Odena G, et al. Hepatic lipocalin 2 promotes liver fibrosis and portal hypertension. Sci Rep. 2020;10(1):15558. doi:10.1038/s41598-020-72172-7

S11. Rokni M, Sadeghi Shaker M, Kavosi H, Shokoofi S, Mahmoudi M, Farhadi E. The role of endothelin and RAS/ERK signaling in immunopathogenesis-related fibrosis in patients with systemic sclerosis: an updated review with therapeutic implications. Arthritis Res Ther. 2022;24(1):108. doi:10.1186/s13075-022-02787-w

S12. Kostov K. The Causal Relationship between Endothelin-1 and Hypertension: Focusing on Endothelial Dysfunction, Arterial Stiffness, Vascular Remodeling, and Blood Pressure Regulation. Life (Basel). 2021;11(9):986. doi:10.3390/life11090986

S13. Granger JP, Spradley FT, Bakrania BA. The Endothelin System: A Critical Player in the Pathophysiology of Preeclampsia. Curr Hypertens Rep. 2018;20(4):32. doi:10.1007/s11906-018-0828-4

S14. Kwiatkowska E, Stefańska K, Zieliński M, et al. Podocytes-The Most Vulnerable Renal Cells in Preeclampsia. Int J Mol Sci. 2020;21(14):5051. doi:10.3390/ijms21145051

S15. Tocci P, Blandino G, Bagnato A. YAP and endothelin-1 signaling: an emerging alliance in cancer. J Exp Clin Cancer Res. 2021;40(1):27. doi:10.1186/s13046-021-01827-8

S16. Dashwood MR, Loesch A. Endothelin-1, endothelin receptor antagonists, and vein graft occlusion in coronary artery bypass surgery: 20 years on and still no journey from bench to bedside. Can J Physiol Pharmacol. 2020;98(9):570-578. doi:10.1139/cjpp-2019-0598

S17. Juif PE, Dingemanse J, Ufer M. Clinical Pharmacology of Clazosentan, a Selective Endothelin A Receptor Antagonist for the Prevention and Treatment of aSAH-Related Cerebral Vasospasm. Front Pharmacol. 2020;11:628956. doi:10.3389/fphar.2020.628956

S18. Khezri MR, Varzandeh R, Ghasemnejad-Berenji M. The probable role and therapeutic potential of the PI3K/AKT signaling pathway in SARS-CoV-2 induced coagulopathy. Cell Mol Biol Lett. 2022;27(1):6. doi:10.1186/s11658-022-00308-w

S19. Acharya A, Pathania AS, Pandey K, et al. PI3K-α/mTOR/BRD4 inhibitor alone or in combination with other anti-virals blocks replication of SARS-CoV-2 and its variants of concern including Delta and Omicron. Clin Transl Med. 2022;12(4):e806. doi:10.1002/ctm2.806

S20. Fattahi S, Khalifehzadeh-Esfahani Z, Mohammad-Rezaei M, Mafi S, Jafarinia M. PI3K/Akt/mTOR pathway: a potential target for anti-SARS-CoV-2 therapy. Immunol Res. Published online February 2, 2022. doi:10.1007/s12026-022-09268-x

S21. Perpiñan C, Bertran L, Terra X, et al. Resistin and IL-15 as Predictors of Invasive Mechanical Ventilation in COVID-19 Pneumonia Irrespective of the Presence of Obesity and Metabolic Syndrome. J Pers Med. 2022;12(3):391. doi:10.3390/jpm12030391

S22. Ling L, Chen Z, Lui G, et al. Longitudinal Cytokine Profile in Patients With Mild to Critical COVID-19. Front Immunol. 2021;12:763292. doi:10.3389/fimmu.2021.763292

S23. Pérez-García F, Martin-Vicente M, Rojas-García RL, et al. High SARS-CoV-2 Viral Load and Low CCL5 Expression Levels in the Upper Respiratory Tract Are Associated With COVID-19 Severity. J Infect Dis. 2022;225(6):977-982. doi:10.1093/infdis/jiab604

S24. Saheb Sharif-Askari F, Goel S, Saheb Sharif-Askari N, et al. Asthma Associated Cytokines Regulate the Expression of SARS-CoV-2 Receptor ACE2 in the Lung Tissue of Asthmatic Patients. Front Immunol. 2021;12:796094. doi:10.3389/fimmu.2021.796094

S25. Jessop F, Schwarz B, Scott D, et al. Impairing RAGE signaling promotes survival and limits disease pathogenesis following SARS-CoV-2 infection in mice. JCI Insight. 2022;7(2):e155896. doi:10.1172/jci.insight.155896

S26. Kovács D, Fazekas F, Oláh A, Törőcsik D. Adipokines in the Skin and in Dermatological Diseases. Int J Mol Sci. 2020;21(23):E9048. doi:10.3390/ijms21239048

S27. Miltiades A, Houck PJ, Monteleone M, et al. Insights into Fibrinogen-Mediated COVID-19 Hypercoagubility in Critically Ill Patients. J Neurosurg Anesthesiol. 2022;34(1):136-140. doi:10.1097/ANA.0000000000000812

S28. Borella R, De Biasi S, Paolini A, et al. Metabolic reprograming shapes neutrophil functions in severe COVID-19. Eur J Immunol. 2022;52(3):484-502. doi:10.1002/eji.202149481

S29. Corallo C, Pinto AM, Renieri A, et al. Altered expression of RXFP1 receptor contributes to the inefficacy of relaxin-based anti-fibrotic treatments in systemic sclerosis. Clin Exp Rheumatol. 2019;37 Suppl 119(4):69-75.

S30. Khan MAAK, Islam ABMMK. SARS-CoV-2 Proteins Exploit Host's Genetic and Epigenetic Mediators for the Annexation of Key Host Signaling Pathways. Front Mol Biosci. 2020;7:598583. doi:10.3389/fmolb.2020.598583

S31. Bordoni V, Matusali G, Mariotti D, et al. The interplay between SARS-CoV-2 infected airway epithelium and immune cells modulates regulatory/inflammatory signals. iScience. 2022;25(2):103854. doi:10.1016/j.isci.2022.103854